

# Spectral Bias in Adaptive Beamforming with Narrowband Interference

Brian D. Jeffs, *Senior Member, IEEE*, and Karl F. Warnick *Senior Member, IEEE*

**Abstract**—It is shown that adaptive canceling arrays which track interference by regular updates of the beamformer weights can introduce a spectral null at the excited interference frequency. This PSD estimation bias effect we call “spectral scooping” is most prominent for narrowband interference (i.e. occupying only a few spectral bins at the desired PSD estimation resolution). Scooping is problematic in radio astronomy where bias in either the weak signal or noise floor spectra can corrupt the observation. The mathematical basis for scooping is derived, and an algorithm to eliminate it is proposed. Both simulated and real data experiments demonstrate the effectiveness of the proposed algorithm.

**Index Terms**—Adaptive arrays, Interference suppression, Radio Astronomy, Spectral analysis

## I. INTRODUCTION

### A. Background

This paper considers using a sensor array to form a power spectral density (PSD) estimate for a signal of interest (SOI) in the presence of strong narrowband interference. We assume the processing architecture of Figure 1. Though the problem is general, our motivation arises from radio astronomy (RA) observation, where the SOI is very weak and there is frequently disabling man-made interference. The array could be a set of many separate bare antennas as proposed for some new large RA instruments such as LOFAR [1]–[3], or a compact array used as an adaptive feed at the focal point of a large dish telescope, as under study for the Green Bank Telescope [4]–[8]

We will show that adaptive array interference cancellation can have an undesired effect of over-canceling to the point of notching out the baseline noise or SOI spectrum. This phenomenon which we have dubbed “spectral scooping” can be seen in Figures 2, 3, 6, and 7 in following sections. In these examples, interference has been effectively cancelled by the adaptive spatial filter, but so has some of the noise and signal spectrum at the same frequencies.

The problem is more prevalent when interference, even transiently, has a strong very narrowband component (spanning only a few PSD estimation bin widths) as may be encountered with some navigational beacons, pilot tones, dominant carriers during quiet passages in AM modulation, and a variety of other modulation schemes. The scooping behavior does not occur when adaptive beamforming weights are computed from exact array covariance matrices, but it will be shown that sample estimation error terms induce a coupling between a strong

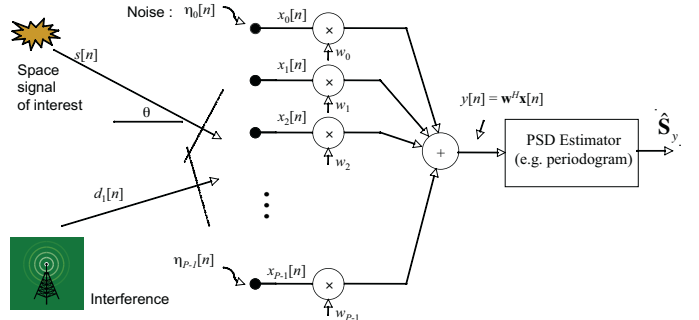


Fig. 1. Block diagram of the basic array PSD estimation system.

interferer and noise plus SOI which causes this unexpected notch in the desired PSD.

Of course, placing a null in the PSD biases the estimate and can be as problematic as is incomplete interference canceling. For radio astronomy, cancellation biases have been a source of astronomers’ reluctance to adopt adaptive beamforming techniques [9]–[11]. The focus of this paper is understanding the causes of spectral scooping, and presenting a solution.

The remainder of the paper is organized as follows. Section I-B and I-C describe mathematical models for the sensor array and array processing and spectral estimation architectures. Section II defines the “spectral scooping” effect which is the central subject of this paper, provides an approximate analysis of its origin, and introduces a proposed algorithm to mitigate the effect. Section III presents both simulated and real data experimental results to demonstrate spectral scooping and performance of the proposed mitigation algorithm. Conclusions and observations are found in Section IV. Finally, extended derivations, mathematical notation, operators, and function definitions are provided in the Appendix.

### B. Signal Model

Consider the  $P$  element sensor array of Figure 1, which produces a length  $P \times 1$  complex baseband sample data vector

$$\mathbf{x}[n] = \mathbf{a}s[n] + \sum_{q=1}^Q \mathbf{v}_q[n]d_q[n] + \boldsymbol{\eta}[n] \quad (1)$$

where  $s[n]$  is the SOI,  $\boldsymbol{\eta}[n]$  is noise, and  $d_q[n]$  is one of  $Q$  “detrimental” interfering sources. Vectors  $\mathbf{a}$  and  $\mathbf{v}_q[n]$  are normalized array spatial responses to  $s[n]$  and  $d_q[n]$  respectively. Assume that  $s[n]$ ,  $d_q[n]$ , and  $\boldsymbol{\eta}[n]$  are mutually independent wide sense stationary zero mean random processes with variances  $\sigma_s^2$ ,  $\sigma_{d_q}^2$ , and covariance  $\sigma_\eta^2 \mathbf{I}$  respectively. Assume  $s[n]$  is spatially fixed, so  $\mathbf{a}$  is constant. Due to interferer motion,

This work was funded by National Science Foundation under grant number AST - 0352705

Authors are with the Dept. of Elec. and Comp. Eng., Brigham Young University, Provo, UT 84602 USA (bjeffs@ee.byu.edu, warnick@ee.byu.edu).

$\mathbf{v}_q[n]$  varies, but over  $L$  time samples called the ‘‘short term integration (STI)’’ window, it is approximately constant. We will treat  $\mathbf{v}_q[n]$  as a deterministic, though unknown, function of time which depends on interferer motion dynamics and the fixed element spatial response patterns. Examples of such deterministic motion include interference seen at a radio telescope from downlink transmissions of a man-made satellite, or from a fixed ground transmitter where apparent motion is due to telescope re-pointing to track sidereal motion of a deep space source of interest.

The single-complex-weight-per-sensor beamformer architecture of Figure 1 assumes relatively narrowband array operation (or subband processing) such that  $\text{BW} \ll D/c$  where  $\text{BW}$  is the processing bandwidth,  $D$  is the full array aperture diameter, and  $c$  is the speed of wave propagation. At microwave frequencies,  $\text{BW}$  can be as much as 20 MHz or more for a radio astronomical focal plane array. The  $d_q[n]$  are each assumed to occupy only a small fraction of the total  $\text{BW}$ , thus spanning only a few frequency bins at the desired PSD estimator spectral resolution scale. Each interferer may however be at a distinct frequency. This near-single-frequency interference scenario is the condition that leads to spectral scooping during adaptive interference cancellation.

It is desired to estimate the frequency sampled temporal PSD of  $s[n]$  (possibly in combination with the noise PSD) without the corrupting effect of interferers  $d_q[n]$ . One straightforward approach is to compute a beamformer steered to  $s[n]$  followed by a sample PSD estimator, as in Figure 1. Let the beamformer output be

$$y[n] = \mathbf{w}_j^H \mathbf{x}[n], \quad j = \lfloor n/L \rfloor \quad (2)$$

where  $\mathbf{w}_j$  is an adaptive weight vector computed for the  $j$ th STI.

A PSD estimate,  $\hat{S}_y[k]$ , can be formed from  $y[n]$  using Welch’s overlapping windowed averaged periodogram [12],

$$\hat{S}_y[k] = \frac{\gamma}{M} \sum_{m=0}^{M-1} \left| \sum_{n=0}^{N-1} g[n] y[n + m(N - O)] e^{-i2\pi kn/N} \right|^2 \quad (3)$$

where  $g[n]$  is a length  $N$  spectral shaping window (e.g. Hamming). For a fixed beamformer with  $\mathbf{w}_j = \mathbf{w}$ , (3) can be expressed in matrix-vector form as

$$\begin{aligned} \hat{\mathbf{S}}_y^T &= [\hat{S}_y[0], \dots, \hat{S}_y[N-1]] \\ &= \frac{\gamma}{M} \sum_{m=0}^{M-1} |\text{DFT}_N\{\mathbf{y}_m^T \odot \mathbf{g}^T\}|^{\odot 2} \\ &= \frac{\gamma}{M} \sum_{m=0}^{M-1} |\text{DFT}_N\{\mathbf{w}^H \mathbf{X}_m \mathbf{G}\}|^{\odot 2} \\ &= \frac{\gamma}{M} \sum_{m=0}^{M-1} |\mathbf{w}^H \text{DFT}_N\{\mathbf{X}_m \mathbf{G}\}|^{\odot 2}, \quad \text{where} \quad (4) \end{aligned}$$

$$\begin{aligned} \mathbf{y}_m^T &= [y[m(N - O)], \dots, y[m(N - O) + N - 1]] \\ \mathbf{X}_m &= [\mathbf{x}[m(N - O)], \dots, \mathbf{x}[m(N - O) + N - 1]] \\ \mathbf{g} &= [g[0], \dots, g[N - 1]]^T, \quad \mathbf{G} = \text{Diag}\{\mathbf{g}\} \end{aligned}$$

$M$  is the number of DFT averaging windows used,  $O$  is the overlap between successive windows, and the DFT (or

equivalently FFT) operates separately along all matrix rows of its argument. Setting  $\gamma = 1/\text{tr}\{\mathbf{G}\mathbf{G}\}$  properly scales the PSD estimate.

Exploiting stationarity over an STI and assuming spatially white (i.i.d.) noise, define the time dependent array autocorrelation matrix as

$$\begin{aligned} \mathbf{R}_x[n] &= E\{\mathbf{x}[n]\mathbf{x}^H[n]\} \approx \mathbf{R}_{x,j}, \quad j = \lfloor n/L \rfloor \\ \mathbf{R}_{x,j} &= \sigma_s^2 \mathbf{a}\mathbf{a}^H + \sum_{q=1}^Q \sigma_{d_q}^2 \mathbf{v}_{q,j} \mathbf{v}_{q,j}^H + \sigma_\eta^2 \mathbf{I} \end{aligned}$$

where  $\mathbf{v}_{q,j} = \mathbf{v}_q[jL]$ . Signal levels, variances (e.g.  $\sigma_s^2$  and  $\sigma_{d_q}^2$ ), signal to noise ratios (SNR), and interference to noise ratio (INR) in the sequel are defined at sampled complex baseband rather than at the antenna.

The  $L$ -point,  $j$ th STI sample estimator of  $\mathbf{R}_{x,j}$  is

$$\hat{\mathbf{R}}_{x,j} = \frac{1}{L} \sum_{n=jL}^{(j+1)L-1} \mathbf{x}[n]\mathbf{x}^H[n] \quad (5)$$

Note that we do not in general require  $L = N$ , and that unlike the DFT windows, STIs do not overlap.

### C. Subspace Projection Adaptive Beamformer

Beamformer weights,  $\mathbf{w}_j$ , are computed from  $\hat{\mathbf{R}}_{x,j}$  such that interferers will be cancelled while steering a high gain mainlobe toward  $s[n]$ . The beamformer is updated each STI to track interferer motion so that

$$\begin{aligned} \mathbf{w}_j^H \mathbf{V}_j &\approx \mathbf{0} \quad \text{where} \\ \mathbf{V}_j &= [\mathbf{v}_{1,j}, \dots, \mathbf{v}_{Q,j}]. \end{aligned}$$

Any number of algorithms can be considered, including LCMV, MVDR, maximum SNR, and subspace projection spatial filtering [13]–[20]. Though we have observed spectral scooping in each of these mentioned algorithms, in our application we prefer subspace projection since its zero forcing properties often form deeper cancellation nulls. This is particularly desirable in the RA where signals of interest are tens of dB below the noise level, so the following analysis will focus on this architecture. The time-varying (on the STI scale) subspace projection weight vector is computed as

$$\mathbf{w}_j = \hat{\mathbf{P}}_j \mathbf{w} \quad (6)$$

where  $\mathbf{w}$  is a unit length deterministic beamforming weight vector with the desired quiescent (interference-free) response and  $\hat{\mathbf{P}}_j$  is an estimate of  $\mathbf{P}_{\mathbf{V}_j}^\perp$ , the perpendicular subspace projector for  $\mathbf{V}_j$ . When interference dominates, the partitioned SVD approach can be used to compute

$$\hat{\mathbf{P}}_j = \mathbf{I} - \hat{\mathbf{U}}_{d,j} \hat{\mathbf{U}}_{d,j}^H \quad (7)$$

where  $\hat{\mathbf{U}}_{d,j}$  contains the normalized eigenvectors corresponding to the  $Q$  largest eigenvalues in the decomposition  $\hat{\mathbf{R}}_{x,j} = \hat{\mathbf{U}}_j \mathbf{\Lambda} \hat{\mathbf{U}}_j^H$ ,  $\hat{\mathbf{U}}_j = [\hat{\mathbf{U}}_{d,j} | \hat{\mathbf{U}}_{s+\eta,j}]$ , and  $\mathbf{\Lambda}$  is the diagonal matrix of ordered eigenvalues.

## II. SPECTRAL SCOOPING

Causes of spectral scooping are subtle. All cancellation is performed by spatial processing across the channels using  $\mathbf{w}_j$ , which remains constant over an entire STI. However, scooping is a time domain phenomenon that appears in the DFTs used to compute the PSD estimate. The cause is an underlying coupling between the spatial interference canceler and the temporal PSD estimate that arises through the sample STI covariances  $\hat{\mathbf{R}}_{x,j}$ .

We have observed scooping in a wide range of simulated and real data experiments for PSD estimation with an interference canceling array using several adaptive beamforming algorithms. A simplified demonstration program to illustrate scooping behavior is available in [21]. This MATLAB (R) script shows how scooping occurs with both LCMV and subspace projection beamforming, and how the proposed algorithm corrects scooping.

The following section presents an approximation analysis to give insights into why scooping occurs from the perspective of subspace projection beamforming.

### A. Analysis

To illustrate the mathematical basis for scooping, consider a single narrowband interferer at frequency  $\omega_d$ . Figure 3 shows scooping effects for both subspace projection and single constraint LCMV (i.e. MVDR) beamformers.

We assume that

$$\begin{aligned} \sigma_d^2 &\gg \sigma_\eta^2 \gg \sigma_s^2, \\ \sigma_d \sigma_\eta^2 / \sqrt{L} &\gg \sigma_s^2 \end{aligned} \quad (8)$$

These requirements may appear restrictive, but for the radio astronomy application of interest, the signal power is always less than the noise power, and  $\sigma_d^2 \gg \sigma_\eta^2$  is common. Also, the second assumption is usually satisfied with typical parameter values, for example with  $L = 1024$ ,  $\text{INR} = 20$  dB, and  $\text{SNR} = -10$  dB. Scooping can also occur when these assumptions are not strictly satisfied, but these will be used in developing the following approximation analysis which illustrates the genesis of scooping.

Define the SOI plus noise signal  $\mathbf{z}[n] = \mathbf{a}s[n] + \boldsymbol{\eta}[n]$ , so

$$\mathbf{x}[n] = \mathbf{v}_j \sigma_d e^{i\omega_d n} + \mathbf{z}[n], \quad (9)$$

then

$$\mathbf{R}_{x,j} = \mathbf{R}_{d,j} + \mathbf{R}_z = \sigma_d^2 \mathbf{v}_j \mathbf{v}_j^H + \sigma_s^2 \mathbf{a} \mathbf{a}^H + \sigma_\eta^2 \mathbf{I}. \quad (10)$$

Using (9) and (10) in (5), the sample covariance for STI  $j$  can

be expanded as

$$\begin{aligned} \hat{\mathbf{R}}_{x,j} &= \frac{1}{L} \sum_{n=jL}^{(j+1)L-1} \left( \sigma_d^2 \mathbf{v}_j \mathbf{v}_j^H + \sigma_d \mathbf{v}_j e^{i\omega_d n} \mathbf{z}^H[n] \right. \\ &\quad \left. + \sigma_d \mathbf{z}[n] \mathbf{v}_j^H e^{-i\omega_d n} + \mathbf{z}[n] \mathbf{z}^H[n] \right) \\ &= \sigma_d^2 \mathbf{v}_j \mathbf{v}_j^H + \frac{\sigma_d}{L} \mathbf{v}_j \left( \sum_{n=jL}^{(j+1)L-1} \mathbf{z}^H[n] e^{i\omega_d n} \right) \\ &\quad + \frac{\sigma_d}{L} \left( \sum_{n=jL}^{(j+1)L-1} \mathbf{z}[n] e^{-i\omega_d n} \right) \mathbf{v}_j^H \\ &\quad + \sigma_s^2 \mathbf{a} \mathbf{a}^H + \sigma_\eta^2 \mathbf{I} + \mathbf{E}_j \\ &= \mathbf{R}_{d,j} + \frac{\sigma_d}{L} \left( \mathbf{v}_j \mathbf{n}_j^H + \mathbf{n}_j \mathbf{v}_j^H \right) + \mathbf{R}_z + \mathbf{E}_j, \quad \text{where} \end{aligned} \quad (11)$$

$$\mathbf{n}_j = e^{-i\omega_d jL} \sum_{n=0}^{L-1} \mathbf{z}[n + jL] e^{-i\omega_d n} \quad (12)$$

Sample error in the SOI plus noise covariance estimate is expressed by  $\mathbf{E}_j$ , such that

$$\hat{\mathbf{R}}_{z,j} = \frac{1}{L} \sum_n \mathbf{z}[n] \mathbf{z}^H[n] = \mathbf{R}_z + \mathbf{E}_j.$$

Equation (11) indicates that the terms involving  $\mathbf{n}_j$  or  $\mathbf{E}_j$  account for all sample estimation error in  $\hat{\mathbf{R}}_{x,j}$ . They are the only random components in  $\hat{\mathbf{R}}_{x,j}$ . From (12),  $\mathbf{n}_j$  can be recognized as the vector discrete-time Fourier transform for STI window  $j$  of  $\mathbf{z}[n]$ , evaluated at  $\omega = \omega_d$ . As will be shown below, this observation is key to understanding the cause of spectral scooping.

For Gaussian  $s[n]$  and  $\boldsymbol{\eta}[n]$ ,  $L\hat{\mathbf{R}}_{z,j}$  is distributed Wishart, which implies  $E\{\hat{\mathbf{R}}_{z,j}\} = \mathbf{R}_z$ ,  $E\{\mathbf{E}_j\} = \mathbf{0}$ , and  $\text{stdv}\{\mathbf{E}_j\} = \sigma_z^2 / \sqrt{L}$  element-wise, where  $\sigma_z^2 = \sigma_s^2 + \sigma_\eta^2$  [22]. Also, it is easily shown that  $E\{\mathbf{n}_j\} = \mathbf{0}$  and  $\text{stdv}\{\mathbf{n}_j\} = \mathcal{O}(\sqrt{L} \sigma_{z'})$  element-wise, where  $\sigma_{z'}^2 = \sigma_\eta^2 + S_s[k_d]$ . The PSD  $S_s[k_d]$  of  $s[n]$  is evaluated at bin  $k_d$  which contains the interference frequency  $\omega_d$ , so  $\sigma_\eta^2 \leq \sigma_{z'}^2 \leq \sigma_z^2$ , with the upper bound being achieved only if signal and interference have overlapping spectra. Given that they are zero mean, we can use the standard deviations of  $\mathbf{n}_j$  and  $\mathbf{E}_j$  for a fair comparison of relative sizes in their expected contributions to  $\hat{\mathbf{R}}_{x,j}$  with respect to the other deterministic components. Accordingly, an order analysis of terms in  $\hat{\mathbf{R}}_{x,j}$ , taken in sequence as they appear in (11), yields

$$\begin{aligned} \hat{\mathbf{R}}_{x,j} &= \mathcal{O}(\sigma_d^2) + \mathcal{O}\left(\frac{\sigma_d \sigma_{z'}}{\sqrt{L}}\right) + \mathcal{O}(\sigma_\eta^2) \\ &\quad + \mathcal{O}(\sigma_s^2) + \mathcal{O}\left(\frac{\sigma_z^2}{\sqrt{L}}\right) \end{aligned} \quad (13)$$

where the ‘‘order of’’ relationship is taken element-wise in  $\hat{\mathbf{R}}_{x,j}$ . Given the stated assumptions,  $\sigma_d \sigma_{z'} / \sqrt{L}$  is much greater than both  $\sigma_s^2$  and  $\sigma_z^2 / \sqrt{L}$ , so we may neglect the final two terms. Indeed, any combination of signal power levels and  $L$  such that the first two terms dominate the last two will lead to scooping. The third term corresponds to  $\sigma_\eta^2 \mathbf{I}$ , which can also be neglected since its constant diagonal form does not

affect the eigenvectors used to compute projection matrix  $\hat{\mathbf{P}}_j$ . Thus we define  $\check{\mathbf{R}}_{x,j}$  by neglecting all terms in  $\hat{\mathbf{R}}_{x,j}$  which have negligible influence on  $\hat{\mathbf{P}}_j$

$$\check{\mathbf{R}}_{x,j} = \sigma_d^2 \left[ \mathbf{v}_j \mathbf{v}_j^H + \frac{1}{L\sigma_d} \left( \mathbf{v}_j \mathbf{n}_j^H + \mathbf{n}_j \mathbf{v}_j^H \right) \right]. \quad (14)$$

We now exploit this approximation to evaluate the structure of  $\hat{\mathbf{P}}_j$ , as computed from  $\hat{\mathbf{R}}_{x,j}$ . It will be shown that at the interference frequency,  $\hat{\mathbf{P}}_j$  is approximately orthogonal to the combined interference, SOI, and noise signal. This produces a scooping null.

It should be noted that though  $\hat{\mathbf{P}}_j$  and  $\mathbf{n}_j$  are random, the scooping phenomenon occurs per realization. When computing a PSD estimate, these quantities come from the same, single STI window realization of  $\mathbf{x}[n]$ . We have used statistical arguments to assess relative sizes (on average) of terms in  $\hat{\mathbf{R}}_{x,j}$  so negligible components could be dropped to simplify analysis. Now applying these average scale relationships in a single realization, the effect of cross terms (i.e.  $\mathbf{v}_j \mathbf{n}_j^H$ ) which dominate sample estimation error can be studied.

Consider eigenvectors  $\check{\mathbf{u}}_{j,k}$ ,  $k = 1, 2$ , of  $\check{\mathbf{R}}_{x,j}$ , which closely approximate the corresponding dominant eigenvectors  $\hat{\mathbf{u}}_{j,k}$  of  $\hat{\mathbf{R}}_{x,j}$ . In the strong interferer case, the identified interferer subspace is dominated by the two distinct terms in (14). Since  $\mathbf{v}_j$  and  $\mathbf{n}_j$  are the only linearly independent vectors in the expression, the first two eigenvectors of this rank two matrix are seen by inspection to have the form

$$\check{\mathbf{u}}_{j,k} = \mathbf{v}_j + \xi_k \mathbf{n}_j \quad (15)$$

where  $\xi_k$  is a scalar to be determined. It is shown in Appendix A using the approach of [23] that the exact solution for the dominant eigenvector of (14) is given when

$$\xi_1 = \frac{2/(L\sigma_d)}{1 + \sqrt{\left(1 + 2\frac{\text{Re}\{\rho\}}{\alpha}\right)^2 - 4\left(\frac{|\rho|^2}{\alpha^2} + \frac{\beta}{\alpha}\right) - i4\frac{\text{Im}\{\rho\}}{\alpha}}}$$

where  $\alpha = \sigma_d^2 \|\mathbf{v}_j\|^2$ ,  $\beta = \frac{1}{L^2} \|\mathbf{n}_j\|^2$ , and  $\rho = \frac{\sigma_d}{L} \mathbf{v}_j^H \mathbf{n}_j$ .

For strong interference  $\sigma_\eta/\sigma_d \rightarrow 0$ , implying that  $\text{Re}\{\rho\}/\alpha$ ,  $|\rho|/\alpha$ ,  $\beta/\alpha$ , and  $\text{Im}\{\rho\}/\alpha \rightarrow 0$ . So

$$\lim_{\sigma_\eta/\sigma_d \rightarrow 0} \xi_1 = 1/(L\sigma_d)$$

and the dominant eigenvector is

$$\hat{\mathbf{u}}_{j,1} \approx \check{\mathbf{u}}_{j,1} = \mathbf{v}_j + \frac{1}{L\sigma_d} \mathbf{n}_j. \quad (16)$$

Using (7), the projection matrix for interference canceling is  $\hat{\mathbf{P}}_j \approx \mathbf{I} - \check{\mathbf{u}}_{j,1} \check{\mathbf{u}}_{j,1}^H / (\check{\mathbf{u}}_{j,1}^H \check{\mathbf{u}}_{j,1})$ , which, given (16), will be orthogonal to  $\mathbf{v}_j + \mathbf{n}_j / (L\sigma_d)$ .

Now consider the subspace-projection-based PSD estimator for this scenario, and for simplicity use non-overlapping ( $O = 0$ ) DFT windows which match the STI window length (so  $N = L$  and  $m = j$ ), and a rectangular window ( $\mathbf{G} = \mathbf{I}$  and  $\gamma = 1/L$ ). With these parameters, substituting (6) into (4) and using the single interferer and SOI plus noise signal of (9) yields

$$\hat{\mathbf{S}}_y^T = \frac{1}{LM} \sum_{j=0}^{M-1} \left| \mathbf{w}^H \hat{\mathbf{P}}_j^H \text{DFT}_L \left\{ \begin{array}{l} \mathbf{v}_j \sigma_d e^{i\omega_d[n+jL]} \\ + \mathbf{z}[n+jL] \end{array} \right\} \right|^2. \quad (17)$$

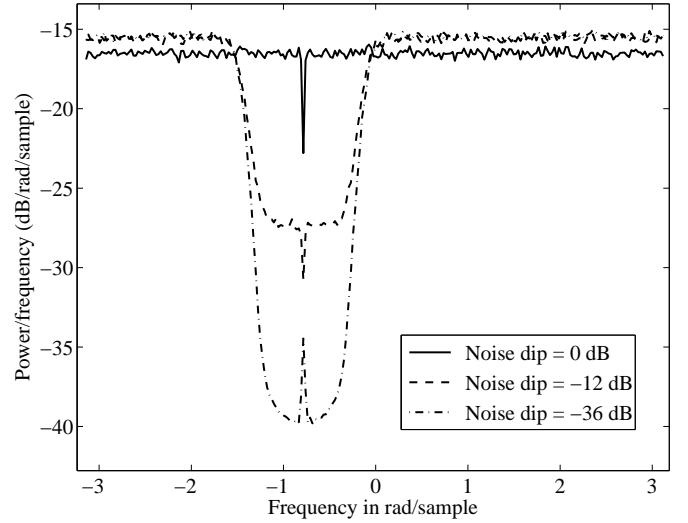


Fig. 2. Spectral scooping and interference leakage effects. For all curves  $\mathbf{z}[n] = \boldsymbol{\eta}[n]$ , i.e. noise only with no SOI. For the solid curve noise is temporally white. For the dashed and dash-dot curves noise is colored, with a dip in the spectrum of -12 and -36 dB respectively near the interference frequency,  $\omega_d = \pi/4$ . Total noise power was the same for all curves. Subspace projection beamforming was used to cancel interference. Note scooping is prominent in the white noise case, and is overwhelmed by interference leakage in the deepest dip case. Total in-band power INR was +10 dB for all curves, the interferer was at  $-60^\circ$  relative to broadside for a seven element  $\lambda/2$  spaced ULA,  $L = N = 256$ , and  $O = 128$ .

where the DFT is over  $0 \leq n \leq L - 1$ . Let  $\omega_k = 2\pi k/N$  be the  $k$ th FFT frequency bin, and pick  $k_d$  such that  $\omega_{k_d} = \omega_d$ , the interference frequency. Then evaluating the DFT in (17) at  $\omega_{k_d}$  and using (12) yields

$$\begin{aligned} \hat{S}_y(k_d) &= \frac{1}{LM} \sum_{j=0}^{M-1} \left| \mathbf{w}^H \hat{\mathbf{P}}_j^H \sum_{n=0}^{L-1} \left( \mathbf{v}_j \sigma_d e^{i\omega_d[n+jL]} + \mathbf{z}[n+jL] \right) e^{-i\omega_d n} \right|^2 \\ &= \frac{1}{LM} \sum_{j=0}^{M-1} \left| \mathbf{w}^H \hat{\mathbf{P}}_j^H \left( L e^{i\omega_d j L} \sigma_d \mathbf{v}_j + e^{i\omega_d j L} \mathbf{n}_j \right) \right|^2 \\ &= \frac{1}{LM} \sum_{j=0}^{M-1} \left| L e^{i\omega_d j L} \sigma_d \right|^2 \left| \mathbf{w}^H \hat{\mathbf{P}}_j^H \left( \mathbf{v}_j + \frac{1}{L\sigma_d} \mathbf{n}_j \right) \right|^2 \\ &= \frac{L\sigma_d^2}{M} \sum_{j=0}^{M-1} \left| \mathbf{w}^H \hat{\mathbf{P}}_j^H \left( \mathbf{v}_j + \frac{1}{L\sigma_d} \mathbf{n}_j \right) \right|^2 \\ &\approx 0 \end{aligned} \quad (18)$$

which is approximately zero due to the orthogonality of  $\hat{\mathbf{P}}_j$  and  $\mathbf{v}_j + \mathbf{n}_j / (L\sigma_d)$ . Therefore a null is placed at  $\omega_d$ , in bin  $k_d$  of  $\hat{\mathbf{S}}_y$ . The desired, interference free PSD bin,  $S_z(k_d)$ , is replaced with a null. At frequencies  $\omega_k \neq \omega_d$ , the noise spectrum term from the DFT in (18) differs from  $\mathbf{n}_j$ , so orthogonality with  $\hat{\mathbf{P}}_j$  is lost and  $S_z(k)$  is properly estimated.

We are aware of one condition where the stated assumptions can be met but scooping will not be apparent. In (14) we have neglected  $\mathbf{E}_j$  using order arguments to simplify analysis, but in practice this term causes an error in  $\hat{\mathbf{P}}_j$  that reduces the interference rejection ratio (IRR). Since cancellation is

not perfect, interference leakage due to  $\mathbf{E}_j$  can “fill in” the scoop null, and even appear as a peak. For scooping to be evident, there must be something to scoop. In other words, the underlying SOI plus noise spectrum  $S_z(k_d)$  must be higher than the residual interference level. Figure 2 illustrates both scooping as predicted by (18), and conditions where the assumptions are satisfied, but interference leakage overwhelms the scoop null. As shown, this does not occur unless the level for  $S_z(\omega)$  is much lower near  $\omega = \omega_d$  than the average level across the band.

To summarize, spectral scooping is caused by some finite sample error terms in  $\hat{\mathbf{R}}_{x,j}$  which appear as a cross correlation between interference and the signal plus noise sequence  $\mathbf{z}[n]$ . The beamformer combines the individual array element data streams so that the residual interference component cancels the other signals present in the interference frequency bin. This result generalizes straightforwardly to other adaptive beamforming algorithms such as LCMV and maximum SNR.

### B. Correcting Spectral Scooping

Consider a subspace projection PSD estimator of the form

$$\hat{\mathbf{S}}_y^T = \frac{1}{LM} \sum_{j=0}^{M-1} \left| \mathbf{w}^H (\hat{\mathbf{P}}_j^a)^H \text{DFT}_L \{ \mathbf{X}_j \} \right|^{\odot 2} \quad (19)$$

where like (17) we have assumed  $L = M$ ,  $O = 0$ , and  $\mathbf{G} = \mathbf{I}$ , but have replaced  $\hat{\mathbf{P}}_j$  with  $\hat{\mathbf{P}}_j^a$  which is computed using only part of the samples in the STI window. Specifically, let  $\mathcal{N}_j = \{n \mid jL \leq n \leq (j+1)L - 1\}$  be the  $L$ -element set of all sample indices in the  $j$ th STI. Partition  $\mathcal{N}_j$  into non-overlapping subsets  $\mathcal{N}_j^a$  and  $\mathcal{N}_j^b$  with  $L_a$  and  $L_b$  elements respectively such that  $\mathcal{N}_j = \mathcal{N}_j^a \cup \mathcal{N}_j^b$ ,  $\mathcal{N}_j^a \cap \mathcal{N}_j^b = \phi$  (the empty set), and  $L = L_a + L_b$ . Sample order is arbitrary. We may then define

$$\hat{\mathbf{R}}_{x,j}^a = \frac{1}{L_a} \sum_{n \in \mathcal{N}_j^a} \mathbf{x}[n] \mathbf{x}^H[n] \quad (20)$$

which is a sample estimate for STI  $j$  computed from an  $L_a$  sample subset of the STI window. Following (15) and Appendix A, it can be shown that  $\hat{\mathbf{R}}_{x,j}^a$  has dominant eigenvector  $\hat{\mathbf{u}}_{j,1}^a \approx \mathbf{v}_j + 1/(L_a \sigma_d) \mathbf{n}_j^a$ , where  $\mathbf{n}_j^a$  is defined as in (12), but summing only over samples  $n \in \mathcal{N}_j^a$ .

Let projection matrix  $\hat{\mathbf{P}}_j^a$  be computed from  $\hat{\mathbf{R}}_{x,j}^a$  as

$$\hat{\mathbf{P}}_j^a = \mathbf{I} - \hat{\mathbf{u}}_{j,1}^a (\hat{\mathbf{u}}_{j,1}^a)^H / ((\hat{\mathbf{u}}_{j,1}^a)^H \hat{\mathbf{u}}_{j,1}^a). \quad (21)$$

It is shown in Appendix B that this projection matrix is closely approximated by

$$\hat{\mathbf{P}}_j^a \approx \mathbf{I} - \tilde{\mathbf{v}}_j \tilde{\mathbf{v}}_j^H - \frac{\mathbf{v}_j (\mathbf{n}_j^a)^H + \mathbf{n}_j^a \tilde{\mathbf{v}}_j^H}{L_a \sigma_d \|\mathbf{v}_j\|}$$

where  $\tilde{\mathbf{v}}_j = \mathbf{v}_j / \|\mathbf{v}_j\|$ . Using  $\hat{\mathbf{P}}_j^a$  in place of  $\hat{\mathbf{P}}_j$  in (18), the

projection product becomes

$$\begin{aligned} \hat{\mathbf{P}}_j^a \left( \mathbf{v}_j + \frac{1}{L \sigma_d} \mathbf{n}_j \right) &\approx \\ &\left( \mathbf{I} - \tilde{\mathbf{v}}_j \tilde{\mathbf{v}}_j^H - \frac{\mathbf{v}_j (\mathbf{n}_j^a)^H + \mathbf{n}_j^a \tilde{\mathbf{v}}_j^H}{L_a \sigma_d \|\mathbf{v}_j\|} \right) \left( \mathbf{v}_j + \frac{1}{L \sigma_d} \mathbf{n}_j \right) \\ &= \mathbf{v}_j - \mathbf{v}_j - \frac{\mathbf{n}_j^a}{L_a \sigma_d} + \frac{\mathbf{n}_j^a + \mathbf{n}_j^b}{L \sigma_d} - \frac{\tilde{\mathbf{v}}_j^H \mathbf{n}_j}{L \sigma_d} \tilde{\mathbf{v}}_j \\ &\quad - \frac{(\mathbf{n}_j)^H \tilde{\mathbf{v}}_j}{L_a \sigma_d} \tilde{\mathbf{v}}_j - \frac{(\tilde{\mathbf{v}}_j^H \mathbf{n}_j) \mathbf{n}_j^a + ((\mathbf{n}_j^a)^H \mathbf{n}_j) \mathbf{v}_j}{L_a L \sigma_d^2 \|\mathbf{v}_j\|} \\ &\approx \frac{\mathbf{n}_j^b - \frac{L_b}{L_a} \mathbf{n}_j^a - \left( \tilde{\mathbf{v}}_j^H \mathbf{n}_j + \frac{L}{L_a} (\mathbf{n}_j^a)^H \tilde{\mathbf{v}}_j \right) \tilde{\mathbf{v}}_j}{L \sigma_d} \end{aligned} \quad (22)$$

where we have used  $\mathbf{n}_j = \mathbf{n}_j^a + \mathbf{n}_j^b$ ,  $L - L_a = L_b$ , and the final term from the previous line was dropped in (22) due to division by large  $L_a L$ .

Substituting (22) into (18) and taking expectation yields

$$\begin{aligned} E\{\hat{S}_y(k_d)\} &\approx \frac{1}{LM} \sum_{j=0}^{M-1} E \left\{ \left| \mathbf{w}^H \mathbf{n}_j - \frac{L_b}{L_a} \mathbf{w}^H \mathbf{n}_j^a \right. \right. \\ &\quad \left. \left. - \left( \tilde{\mathbf{v}}_j^H \mathbf{n}_j + \frac{L}{L_a} (\mathbf{n}_j^a)^H \tilde{\mathbf{v}}_j \right) \mathbf{w}^H \tilde{\mathbf{v}}_j \right|^2 \right\} \\ &\approx \frac{1}{LM} \sum_{j=0}^{M-1} E \left\{ \left| \mathbf{w}^H \mathbf{n}_j - \frac{L_b}{L_a} \mathbf{w}^H \mathbf{n}_j^a \right|^2 \right\} \\ &\approx \frac{1}{LM} \sum_{j=0}^{M-1} \mathbf{w}^H E \{ \mathbf{n}_j (\mathbf{n}_j)^H \} \mathbf{w} + \\ &\quad \frac{L_b^2}{L_a^2} \mathbf{w}^H E \{ \mathbf{n}_j^a (\mathbf{n}_j^a)^H \} \mathbf{w} \\ &\approx \frac{1}{LM} \sum_{j=0}^{M-1} \mathbf{w}^H \mathbf{w} L_b \sigma_{z'}^2 + \mathbf{w}^H \mathbf{w} \frac{L_b^2}{L_a} \sigma_{z'}^2 \\ &\approx \frac{L_b}{L_a} \sigma_{z'}^2 = \frac{L - L_a}{L_a} \sigma_{z'}^2, \quad 0 < L_a \leq L. \end{aligned} \quad (23)$$

The second line follows because  $\mathbf{w}^H \tilde{\mathbf{v}}_j$  is small. Note that  $\|\mathbf{w}\| = \|\tilde{\mathbf{v}}_k\| = 1$  and  $\tilde{\mathbf{v}}_j$  is the normalized array response vector for the interferer. Thus in the typical scenario where the interferer is observed in the sidelobe pattern of the quiescent beamformer,  $\mathbf{w}^H \tilde{\mathbf{v}}_j$  is 20 dB or more below the mainlobe response. In line three we have assumed  $\mathbf{n}_j^a$  and  $\mathbf{n}_j^b$  are uncorrelated. This is not strictly true since they represent Fourier transforms of disjoint sample sets of  $\mathbf{z}[n] = \mathbf{a}s[n] + \boldsymbol{\eta}[n]$ . Typically  $s[n]$  is colored, and though  $\boldsymbol{\eta}[n]$  dominates in  $\mathbf{z}[n]$ , we have not assumed it is temporally white. However, in the usual scenario the correlation time of  $z[n]$  is much less than large  $L$ , so choosing  $\mathcal{N}_j^a$  and  $\mathcal{N}_j^b$  as non-interleaved sets (e.g. first and last halves of the STI window respectively) yields highly uncorrelated  $\mathbf{n}_j^a$  and  $\mathbf{n}_j^b$ . Line four exploits spatially i.i.d. noise across array elements, and the fact that  $E\{|\mathbf{n}_j^a|^2\} = L_a \sigma_{z'}^2$ , and  $E\{|\mathbf{n}_j^b|^2\} = L_b \sigma_{z'}^2$ . Line five relies on  $\|\mathbf{w}\| = 1$  and some algebra.

For  $L_a = L_b = L/2$  the estimator in (23) is approximately unbiased by interference scooping, with  $E\{\hat{S}_y(k_d)\} = \sigma_{z'}^2$ .

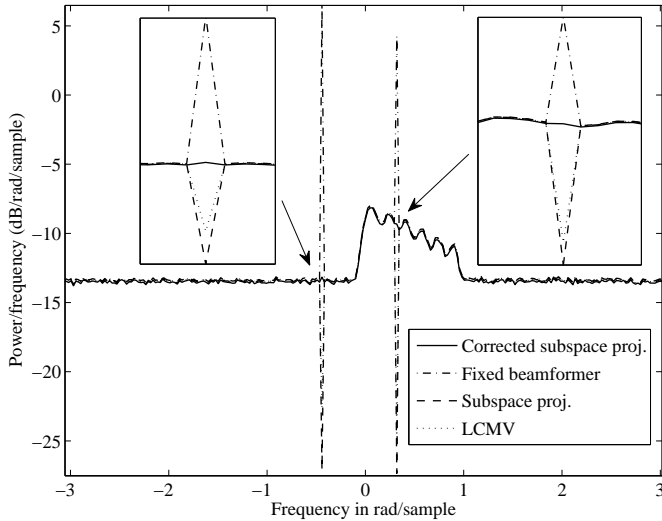


Fig. 3. Spectral scooping and the correction algorithm. Narrowband interferers are at  $\omega \approx -0.5$  and  $\omega \approx 0.3$ , each with +10 dB INR relative to total in-band noise power. The sawtooth shaped SOI is at  $0 \leq \omega \leq 1$ . Conventional beamforming did not cancel interference. Subspace projection and LCMV beamformers both show significant spectral scooping, though typically the LCMV null is not quite as deep. Insets show detail of the corrected PSD.

Note that  $\sigma_z^2$  is the desired SOI plus noise PSD at  $\omega_d$ . This is the basis for our proposed algorithm to eliminate scooping. On the other hand, for  $L_a = L$ ,  $L_b = 0$ ,  $E\{\hat{S}_y(k_d)\} = 0$ , which is the full scooping case predicted by (18). A residual interference peak corrupts the PSD when  $L_a < L/2$ . These behaviors predicted by (23) are verified in simulation experiments presented below.

The scooping bias corrected estimator has the disadvantage that only half of the data is used in forming the adaptive beamformer weight,  $\mathbf{w}_j$  (though all data is used in the DFT computation). Thus  $\mathbf{w}_j$  has increased estimation error jitter. The following algorithm partially mitigates this limitation and uses all the data to compute projections matrices. Let  $\mathcal{N}_j^a$  contain the first  $L/2$ , and  $\mathcal{N}_j^b$  the last  $L/2$  sample indices in STI  $j$ . Form  $\hat{\mathbf{P}}_j^a$  and  $\hat{\mathbf{P}}_j^b$  using  $\hat{\mathbf{R}}_{x,j}^a$  and  $\hat{\mathbf{R}}_{x,j}^b$  computed as in (20) from  $\mathcal{N}_j^a$  and  $\mathcal{N}_j^b$  respectively. Then

$$\hat{\mathbf{s}}_y^T = \frac{\gamma}{2M} \sum_{m=0}^{M-1} \left( \left| \mathbf{w}^H \hat{\mathbf{P}}_j^a \text{DFT}_N \{ \mathbf{X}_m \mathbf{G} \} \right|^{\odot 2} + \left| \mathbf{w}^H \hat{\mathbf{P}}_j^b \text{DFT}_N \{ \mathbf{X}_m \mathbf{G} \} \right|^{\odot 2} \right) \quad (24)$$

$$j = \lfloor m(N - O)/L \rfloor$$

where we have allowed STI and FFT windows to be of unequal length, and FFT windows to overlap.

### III. RESULTS

#### A. Simulation Experiments

Figure 3 presents a computer simulated scenario using a  $P = 7$  element uniform line array with half wavelength spacing. The SOI is located at an azimuth of  $5^\circ$  with a peak (across frequency) signal to noise ratio of 5 dB. The SOI is a Gaussian narrowband random process with a PSD

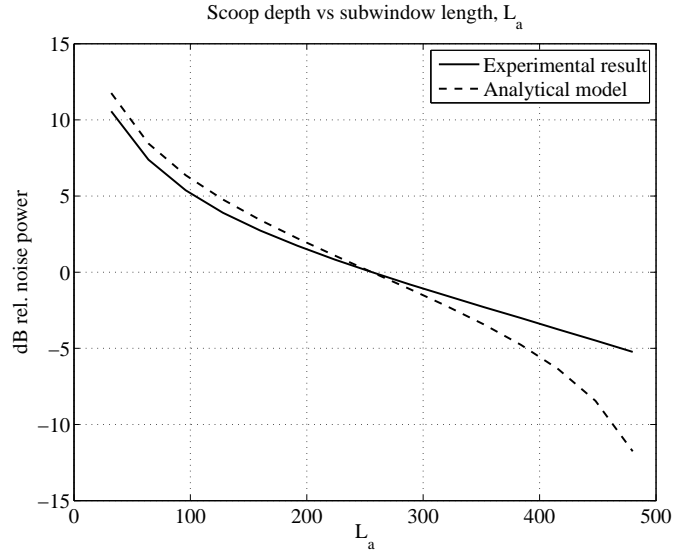


Fig. 4. Scooping depth in the interference frequency bin as a function of STI window subset size,  $L_a$ . Plots are relative to the desired PSD estimate of the true noise floor PSD level. No SOI is present. Negative dB values indicate a scoop; positive values show incomplete interference cancellation. The “analytical model” curve is for equation (23), and the “experimental result” is obtained with 100 Monte Carlo trials of subspace projection array PSD estimates for each value of  $L_a$ . STI window length was  $L = 512$ .

shaped by bandpass filtering, and appears as a declining ramp structure with scalloped top in the figures. Two moving narrowband interferers were present, one inside the SOI band, and one outside. The initial azimuths were  $-60^\circ$  and  $70^\circ$ , with angular rates of  $2 \times 10^{-5}$  and  $-6 \times 10^{-5}$  degrees per sample respectively. A total of  $5 \times 10^5$  samples were used, with non-overlapping STIs of length  $L = 256$  and rectangularly windowed ( $\mathbf{G} = \mathbf{I}$ ) FFTs of length  $N = 256$ . Scooping is clearly evident in the subspace projection beamformer, distorting both the noise floor and SOI PSD estimates. The algorithm of (24) was used to obtain the corrected curve, which completely eliminates scooping while fully canceling the interferer. Similar results (not shown) were obtained with the LCMV beamformer by using  $\hat{\mathbf{R}}_{x,j}^a$  alone in computing  $\mathbf{w}_j$ .

Figure 4 compares the scoop depth predicted by (23) with numerical results from 100 Monte Carlo trials. In the simulations the subspace projection PSD estimator of (19) was used with  $\hat{\mathbf{P}}_j^a$  computed from STI subwindows of varying length,  $L_a$ . A single stationary interferer at  $-60^\circ$  was observed with 20 dB INR at the 7 element,  $\lambda/2$  spaced uniform line array. STI length  $L$  and FFT window length  $N$  were both 512, with FFT windows overlapped 50%.

Good agreement between the curves is found until  $L_a \rightarrow L$ , at which point (23) over-predicts scoop depth due to approximations made in the analysis. Interferer leakage, or equivalently low IRR, due the  $\mathbf{E}_j$  error term is not taken into account in the approximate analysis. However, both curves cross 0 dB (i.e. no scooping bias) as predicted for  $L_a = L/2 = 256$ .



(a)



(b)

Fig. 5. The array feed test platform. a) Feed array mounted on three meter dish reflector. b) Close up of seven element feed.

### B. Real Data Experiments

This section presents results from an experiment with a seven element L-band ( $\approx 1600$  MHz) array feed mounted at the focal plane of a three meter diameter parabolic dish. This test platform at Brigham Young University (BYU) is used for rapid prototyping to study signal processing algorithms for radio astronomy. Figure 5 shows the antenna system and hexagonal array feed. The inter-element spacing of 0.6 wavelength provides a “fully sampled” array [4], [24]. Development of the BYU array is reported in [6], [25].

Figures 6 and 7 presents PSD estimation results for a real data experiment. Array signals were acquired by a seven channel analog receiver, digitized at 1.25 Msamp/sec/channel, and streamed to disk for post processing. The SOI and interference signals were from CW microwave function generators with antennas located on neighboring buildings. The SOI was seen at boresight and the moving interferer was seen in the dish sidelobe pattern at approximately  $30^\circ$  azimuth. Interference-to-signal power ratio was 113 dB at the sources, but the interferer was approximately three times further from the

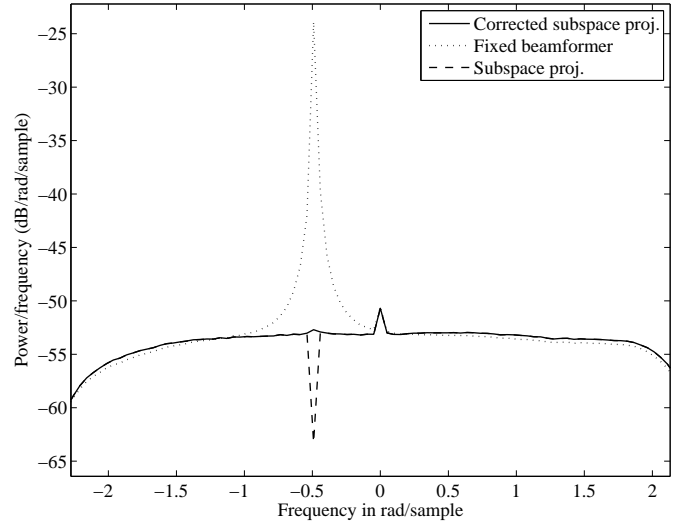


Fig. 6. Real data experiment for a 7 element array feed and 3m dish. The SOI is at  $\omega = 0.0$ , corresponding to 1571.3 MHz. The 1571.35 MHz interferer appears at  $\omega = -0.5$ . Note the 10 dB deep subspace projection scoping null, which is eliminated by the proposed algorithm.

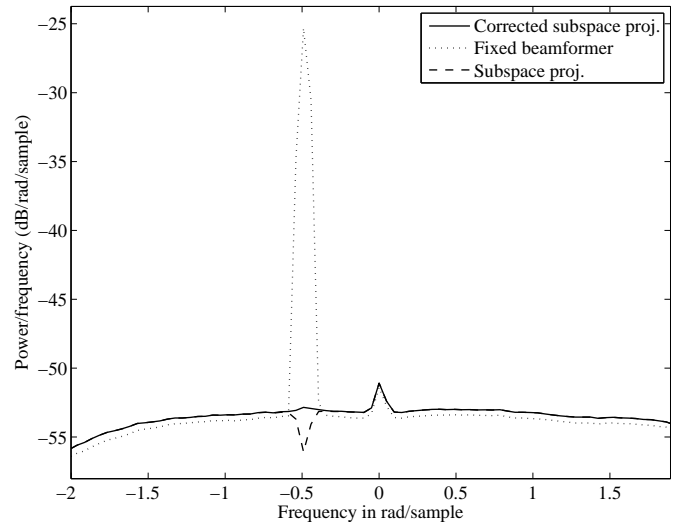


Fig. 7. Scoping for the seven-element array feed using 50% overlapping windows, and Hamming window shaping for the FFT calculations. Note that scoping is less prominent than the non-overlapping, rectangular windowed case of Figure 6 for the same data samples, but the proposed algorithm still improves the PSD estimate.

dish than was the SOI. Data was processed using (24), with length  $L = N = 128$  non-overlapping rectangular windows. Additional physical details for the experiment are found in [26].

Figure 6 clearly demonstrates that spectral scoping does in fact occur in real adaptive cancellation scenarios. We observed scoping in virtually all of our real sample data with narrowband interference, and even in some relatively broadband FM interference cases. The proposed algorithm effectively corrects the PSD bias. In cases (as in the figure) where a small residual interference “leak through” occurs, its height is typically less than the original scoping null depth. Figure 7 shows how a tapered spectral shaping window (e.g. Hamming)

does reduce scooping depth when compared to using the rectangular window which was assumed in the analysis of Section II.

#### IV. CONCLUSIONS

We have demonstrated, both mathematically and experimentally, the existence of previously unknown PSD estimation bias which we have dubbed “spectral scooping.” This null in the signal plus noise spectrum occurs while using adaptive array beamforming to spatially cancel an interferer who’s bandwidth is spans just a few frequency bins of the PSD estimator. Though beamformer weights operate on the array spatial response and are not generally considered capable of affecting the temporal-spectral content of a signal, the fact that weights are updated periodically with a data dependent calculation opens an avenue for modification of the estimated spectrum. It was shown that scooping is an artifact of estimation error in the short-term integration (STI) sample covariance matrix. This sample error includes cross product terms between interference and noise plus signal which couple into the PSD estimator. Scooping does not occur when adaptive beamformer weights are computed from snapshot exact covariance matrices, even for time-varying interference spatial signatures.

A correction algorithm was introduced that exploits a specific relationship between the scoop depth and the percentage of samples in the covariance estimation window which are used to calculate beamformer weights,  $\mathbf{w}_j$ . We have found that scoop depth is reduced (though not eliminated) when tapering windows are used for  $\mathbf{G}$ , when  $L \neq N$ , and when  $O \neq 0$  so DFT widows overlap. We recommend using these parameter settings in conjunction with the proposed correction algorithm.

Scooping is problematic only in a somewhat specialized observing scenario, i.e. with *i*) quite narrowband interference, *ii*) regularly updated spatial adaptive filtering, *iii*) specific relationships for the various signal powers and STI length as in (8), and *iv*) when a spectral notch in the SOI is detrimental to signal processing goals. However, these conditions do arise in real-world scenarios, and we have encountered them repeatedly in realistic radio astronomical observing situations. The effect is surprising, and we believe practitioners of array signal processing should be aware if its potential corruption to their experiments and applications which use canceling array beamformers.

A simple demonstration code is available at [21] for readers to familiarize themselves with the scooping phenomenon and operation of the proposed correction algorithm.

#### APPENDIX

##### A. Exact Eigen Solution for a Rank Two STI Covariance

The first two eigenvectors of (14) are seen by inspection of to have the form

$$\check{\mathbf{u}}_{j,k} = \mathbf{v}_j + \xi_k \mathbf{n}_j, \quad k = 1, 2. \quad (25)$$

The exact solution for the dominant eigenvector of  $\check{\mathbf{R}}_{x,j}$  is found as follows [23]. Using (16), the eigen equation can be

expressed as

$$\begin{aligned} \lambda \check{\mathbf{u}}_j &= \check{\mathbf{R}}_{x,j} \check{\mathbf{u}}_j \\ \lambda (\mathbf{v}_j + \xi \mathbf{n}_j) &= \left[ \sigma_d^2 \mathbf{v}_j \mathbf{v}_j^H + \frac{\sigma_d}{L} (\mathbf{v}_j \mathbf{n}_j^H + \mathbf{n}_j \mathbf{v}_j^H) \right] \\ &\quad \times (\mathbf{v}_j + \xi \mathbf{n}_j) \\ \lambda \mathbf{v}_j + \lambda \xi \mathbf{n}_j &= \left( \alpha + \rho^* + (\rho + \beta) L \sigma_d \xi \right) \mathbf{v}_j \\ &\quad + \left( \frac{\alpha}{L \sigma_d} + \rho \xi \right) \mathbf{n}_j \end{aligned}$$

Where  $\alpha = \sigma_d^2 \|\mathbf{v}_j\|^2$ ,  $\beta = \frac{1}{L^2} \|\mathbf{n}_j\|^2$ , and  $\rho = \frac{\sigma_d}{L} \mathbf{v}_j^H \mathbf{n}_j$ . Matching coefficients of  $\mathbf{v}_j$  and  $\mathbf{n}_j$  respectively and solving for  $\lambda$  yields the two equations

$$\begin{aligned} \lambda &= \alpha + \rho^* + (\rho + \beta) L \sigma_d \xi, \text{ and} \\ \lambda &= \frac{\alpha}{L \sigma_d \xi} + \rho. \end{aligned}$$

Thus  $L \sigma_d \xi = \frac{\alpha}{\lambda - \rho}$ , which when substituted into the first equation leads to

$$\lambda^2 - (\alpha + \rho^* + \rho) \lambda - \alpha \beta + |\rho|^2 = 0.$$

This is solved with the quadratic formula to yield

$$\lambda = \frac{\alpha + 2\text{Re}\{\rho\} \pm \sqrt{(\alpha + 2\text{Re}\{\rho\})^2 - 4(|\rho|^2 - \alpha\beta)}}{2}.$$

Substituting this result into  $\xi = \frac{\alpha}{L \sigma_d (\lambda - \rho)}$  and taking the positive radical term produces the needed parameter to determine the dominant eigenvector:

$$\xi_1 = \frac{2/(L \sigma_d)}{1 + \sqrt{\left(1 + 2 \frac{\text{Re}\{\rho\}}{\alpha}\right)^2 - 4 \left(\frac{|\rho|^2}{\alpha^2} + \frac{\beta}{\alpha}\right)} - i 4 \frac{\text{Im}\{\rho\}}{\alpha}}$$

##### B. Projection Matrix for Partial STI Window

We find a closed form close approximation for the projection matrix computed from a sub-window of  $L_a$  samples from STI  $j$ . Compute the dominant eigenvector,  $\hat{\mathbf{u}}_{j,1}^a$ , for  $\check{\mathbf{R}}_{x,j}^a$ . Let  $\hat{\mathbf{P}}_j^a = \mathbf{I} - \hat{\mathbf{u}}_{j,1}^a (\hat{\mathbf{u}}_{j,1}^a)^H / ((\hat{\mathbf{u}}_{j,1}^a)^H \hat{\mathbf{u}}_{j,1}^a)$ , which by substituting from (16) can be expanded as

$$\begin{aligned} \hat{\mathbf{P}}_j^a &\approx \mathbf{I} - \frac{(\mathbf{v}_j + \frac{1}{L \sigma_d} \mathbf{n}_j^a)(\mathbf{v}_j + \frac{1}{L \sigma_d} \mathbf{n}_j^a)^H}{\|\mathbf{v}_j + \frac{1}{L \sigma_d} \mathbf{n}_j^a\|^2} \\ &\approx \mathbf{I} - \frac{(\mathbf{v}_j + \frac{1}{L \sigma_d} \mathbf{n}_j^a)(\mathbf{v}_j + \frac{1}{L \sigma_d} \mathbf{n}_j^a)^H}{\|\mathbf{v}_j\|^2} \\ &\approx \mathbf{I} - \frac{\mathbf{v}_j \mathbf{v}_j^H}{\|\mathbf{v}_j\|^2} - \frac{\mathbf{n}_j^a \mathbf{v}_j^H}{L_a \sigma_d \|\mathbf{v}_j\|^2} \\ &\quad - \frac{\mathbf{v}_j (\mathbf{n}_j^a)^H}{L_a \sigma_d \|\mathbf{v}_j\|^2} - \frac{\mathbf{n}_j^a (\mathbf{n}_j^a)^H}{L_a^2 \sigma_d^2 \|\mathbf{v}_j\|^2} \\ \hat{\mathbf{P}}_j^a &\approx \mathbf{I} - \tilde{\mathbf{v}}_j \tilde{\mathbf{v}}_j^H - \frac{\mathbf{v}_j (\mathbf{n}_j^a)^H + \mathbf{n}_j^a \tilde{\mathbf{v}}_j^H}{L_a \sigma_d \|\mathbf{v}_j\|} \end{aligned}$$

where  $\tilde{\mathbf{v}}_j = \mathbf{v}_j / \|\mathbf{v}_j\|$  and in the final approximation the last term was neglected since it is very small due to division by  $L_a^2$ .

### C. Notation

The following notation, operators and identities have been used in the paper:

- 1)  $\mathbf{z}$  : bold, lower case denotes a column vector.
- 2)  $\mathbf{A}$  : bold, upper case denotes a matrix.  $\mathbf{A} = [\mathbf{a}_1, \mathbf{a}_2, \dots, \mathbf{a}_N]$ .
- 3)  $a, B, \alpha$  : italic, non-bold, Roman or Greek denotes a scalar quantity.
- 4)  $\mathbf{I}$  : identity matrix of appropriate size.
- 5)  $i$  :  $= \sqrt{-1}$ .
- 6)  $\mathbf{A}^T$  : transpose of  $\mathbf{A}$ .
- 7)  $\mathbf{A}^*$  : complex conjugate of  $\mathbf{A}$ .
- 8)  $\mathbf{A}^H$  : complex conjugate (Hermitian) transpose of  $\mathbf{A}$ .
- 9)  $|\mathbf{A}|^{\odot 2}$  : element-wise magnitude squared.
- 10)  $\text{diag}\{\mathbf{A}\}$  : extract diagonal of  $\mathbf{A}$  to form a column vector.
- 11)  $\text{Diag}\{\mathbf{z}\}$  : diagonal matrix with  $\mathbf{z}$  appearing along the diagonal.
- 12)  $\text{tr}\{\mathbf{A}\}$  : trace of  $\mathbf{A}$ .
- 13)  $\mathbf{A} \odot \mathbf{B} = \begin{bmatrix} a_{1,1}b_{1,1} & \cdots & a_{1,N}b_{1,N} \\ \vdots & \ddots & \vdots \\ a_{M,1}b_{M,1} & \cdots & a_{M,N}b_{M,N} \end{bmatrix}$ , element-wise, or Hadamard product.
- 14)  $\mathbf{S}_x$  : DFT based power spectral density vector for finite length random sequence  $\mathbf{x}_j$ . This notation is an exception to rule (2).
- 15)  $\text{DFT}_N\{\mathbf{A}\}$  :  $N$  - point discrete Fourier transform along rows of  $M \times N$   $\mathbf{A}$ .
- 16)  $E\{\mathbf{A}\}$  : expected value of random  $\mathbf{A}$ .
- 17)  $\text{stdv}\{X\}$  : standard deviation of  $X$ .
- 18)  $\lfloor a \rfloor$  : floor operation, rounding toward zero.
- 19)  $\hat{\mathbf{A}}$  : estimate of  $\mathbf{A}$ .
- 20)  $\mathcal{O}(\cdot)$  : "on the order of."
- 21)  $\in$  : "is an element of."
- 22)  $\cup, \cap$  : Set union and intersection respectively.

### REFERENCES

- [1] J. E. Noordam, "LOFAR calibration challenges," in *Proceedings of the SPIE, Vol. 5489, pp. 817-825 (2004)*, Oct. 2004, pp. 817-825.
- [2] A.J. Boonstra, S.J. Wijnholds, S. v.d. Tol, and B. Jeffs, "Calibration, sensitivity, and rfi mitigation requirements for lofar," in *Proc. of the IEEE International Conf. on Acoust., Speech, and Signal Processing*, Mar. 2005, vol. V, pp. 869-872.
- [3] S. van der Tol, B.D. Jeffs, and A.-J. van der Veen, "Self calibration for the LOFAR radio astronomical array," *IEEE Transactions on Signal Processing*, vol. 55, no. 9, pp. 4497-4510, Sept. 2007.
- [4] J.R. Fisher and R.F. Bradley, "Full sampling array feeds for radio telescopes," *Proceedings of the SPIE, Radio Telescopes*, vol. 4015, pp. 308-318, 2000.
- [5] Chad K. Hansen, Karl F. Warnick, Brian D. Jeffs, J. Richard Fisher, and Richard Bradley, "Interference mitigation using a focal plane array," *Radio Science*, vol. 40, doi:10.1029/2004RS003138, no. 5, June 2005.
- [6] J.R. Nagel, K.F. Warnick, B.D. Jeffs, J.R. Fisher, and R. Bradley, "Experimental verification of radio frequency interference mitigation with a focal plane array feed," *Radio Science*, vol. 42, 2007, RS6013, doi:10.1029/2007RS003630.
- [7] Bruce Veidt and Peter Dewdney, "A phased-array feed demonstrator for radio telescopes," in *Proc. URSI General Assembly*, 2005.
- [8] R. Maaskant, M. V. Ivashina, R. Mittra, and N. T. Huang, "Parallel FDTD modeling of a focal plane array with Vivaldi elements on the highly parallel LOFAR BlueGene/L supercomputer," in *Proc. IEEE Antennas and Propagation Symposium*, Albuquerque, NM, June 20-25 2006, pp. 3861 - 3864.

- [9] B.D. Jeffs and K.F. Warnick, "Bias corrected psd estimation with an interference canceling array," in *Proc. of the IEEE International Conf. on Acoust., Speech, and Signal Processing*, Honolulu, Apr. 2007, vol. II, pp. 1145-1148.
- [10] S. van der Tol and A.-J. van der Veen, "Performance analysis of spatial filtering of rf interference in radio astronomy," *IEEE Trans. Signal Processing*, vol. 53, no. 3, Mar. 2005.
- [11] A. Leshem and A.-J. van der Veen, "Radio-astronomical imaging in the presence of strong radio interference," *IEEE Trans. Inform. Theory*, vol. 46, no. 5, pp. 1730-1747, Aug. 2000.
- [12] P.D. Welch, "The use of the fast fourier transform for the estimation of power spectra," *IEEE Trans. Audio Electroacoustics*, vol. AU-15, pp. 70-73, June 1970.
- [13] H.L. Van Trees, *Detection, Estimation, and Modulation Theory, Part IV, Optimum Array Processing*, John Wiley and Sons, 2002.
- [14] B.D. Van Veen and K. M. Buckley, "Beamforming: A versatile approach to spatial filtering," *IEEE ASSP Mag.*, pp. 4-24, Apr. 1988.
- [15] A. Leshem, A.-J. van der Veen, and A.-J. Boonstra, "Multichannel interference mitigation techniques in radio astronomy," *Astrophysical Journal Supplements*, vol. 131, no. 1, pp. 355-374, 2000.
- [16] S.W. Ellingson and G.A. Hampson, "A subspace-tracking approach to interference nulling for phased array-based radio telescopes," *IEEE Trans. Antennas Propagat.*, vol. 50, no. 1, pp. 25-30, Jan. 2002.
- [17] H. Cox, "Resolving power and sensitivity to mismatch of optimum array processors," *J. of the Acoustical Soc. of Am.*, vol. ASSP-54, pp. 771-785, Sept. 1973.
- [18] S.P. Applebaum and D.J. Chapman, "Adaptive arrays with main beam constraints," *IEEE Trans. Antennas Propagat.*, vol. AP-24, pp. 650-662, Sept. 1976.
- [19] R.A. Monzingo and T.W. Miller, *Introduction to Adaptive Arrays*, Wiley, New-York, 1980.
- [20] K.M. Buckley, "Spatial/spectral filtering with linearly constrained minimum variance beamformers," *IEEE Trans. Acoust., Speech, Signal Process.*, vol. ASSP-35, pp. 249-266, Mar. 1987.
- [21] B.D. Jeffs, "Demonstration software for 'spectral bias in adaptive beamforming with narrowband interference'," *Tech. note, BYU D-Space*, Jan. 2008, <http://hdl.handle.net/1877/611>.
- [22] D.R. Brillinger, *Time Series: Data Analysis and Theory*, Holt, Rinehart and Winston, New York, 1st edition, 1975.
- [23] B.D. Jeffs, L. Li, and K.F. Warnick, "Auxiliary antenna assisted interference mitigation for radio astronomy arrays," *IEEE Trans. Signal Processing*, vol. 53, no. 2, pp. 439-451, Feb. 2005.
- [24] J.R. Fisher and R.F. Bradley, "Full sampling focal plane array," in *Proceedings of Imaging at Radio Through Millimeter Wavelength Workshop, ASP Conference Series No. 217*, J. Mangum and S.J.E. Radford, Eds., Tucson, AZ, June 1999, pp. 11-18.
- [25] J.R. Nagel, "A prototype platform for array feed development," M.S. thesis, Brigham Young University, 2006, available from BYU electronic thesis collection, <http://etd.byu.edu/collection.html>, <http://contentdm.lib.byu.edu/ETD/image/etd1575.pdf>.
- [26] B.D. Jeffs and K.F. Warnick, "Bias corrected psd estimation for an adaptive array with moving interference," *IEEE Trans. Signal Processing*, vol. 56, pp. doi:10.1109/TSP.2008.919637, 2008.



**Brian D. Jeffs** (M'90-SM'02) received B.S. (magna cum laude) and M.S. degrees in electrical engineering from Brigham Young University in 1978 and 1982 respectively. He received the Ph.D. degree from the University of Southern California in 1989. He is currently an associate professor in the Department of Electrical and Computer Engineering at Brigham Young University, where he lectures in the areas of digital signal processing, digital image processing, and probability theory. Current research interests include array signal processing for radio astronomy,

RF interference mitigation, MIMO wireless communications, and digital image restoration. Previous employment includes Hughes Aircraft Company where he served as a sonar signal processing systems engineer in the anti-submarine warfare group. Dr. Jeffs was a Vice General Chair for IEEE ICASSP-2001, held in Salt Lake City Utah. He was a member of the executive organizing committee for the 1998 IEEE DSP Workshop, and served several years as chair of the Utah Chapter of the IEEE Communications and Signal Processing Societies.



**Karl F. Warnick** (S'95–M'98–SM'04) received the B.S. degree (magna cum laude) with University Honors and the Ph.D. degree from Brigham Young University in 1994 and 1997, respectively. From 1998 to 2000, he was a Postdoctoral Research Associate in the Center for Computational Electromagnetics at the University of Illinois at Urbana-Champaign. Since 2000, he has been a faculty member in the Department of Electrical and Computer Engineering at Brigham Young, where he is currently an Associate Professor. He has authored

a book, *Problem Solving in Electromagnetics, Microwave Circuits, and Antenna Design for Communications Engineering* (Artech House). Research interests include array antenna systems, computational electromagnetics, remote sensing, and inverse scattering. Dr. Warnick was a recipient of the NSF Graduate Research Fellowship, Outstanding Faculty Member award for Electrical and Computer Engineering in 2005, and the BYU Young Scholar Award (2007), and served as Technical Program Co-Chair for the 2007 IEEE International Symposium on Antennas and Propagation.